Macromolecules

pubs.acs.org/Macromolecules Article

Enhanced Crystallinity and Electrical Conductivity in Conjugated Polymers via Dynamic Covalent Bond Exchange

Seongon Jang, Jason L. Wu, Nicholas E. Jackson, Charles M. Schroeder,* and Christopher M. Evans*

Cite This: *Macromolecules* 2026, 59, 9015−9026 Read Online

ACCESS | Metrics & More | Article Recommendations | Supporting Information

ABSTRACT: Conjugated polymers have been extensively used for organic electronics applications due to their tunable optical, electrical, and mechanical properties. Traditional solution-based processing methods for conjugated polymers often require toxic solvents and are limited by polymer solubility. In contrast, solid-state hot pressing offers a straightforward, solvent-free processing method, but subjecting conjugated polymers to temperatures above their melting temperatures T_m can lead to thermal oxidative degradation. Here, we investigate the effect of hot-pressing and acid doping on the crystallinity and electron transport properties of conjugated polymers with dynamic covalent imine bonds between quaterthiophene units (DQT-DP) compared to nondynamic analogs (DQT-NP). Polymers were processed at temperatures below T_m, and enhanced crystallinity was observed using differential scanning calorimetry (DSC) and wide-angle X-ray scattering (WAXS), which is attributed to thermally activated dynamic bond exchange promoting polymer subsegment crystallization and flow-induced interchain $\pi-\pi$ stacking. In contrast, negligible impacts on crystallinity were observed when hot-pressing the nondynamic polymer analog DQT-NP. Enhanced crystallinity in hot-pressed DQT-DP led to higher electrical conductivity after iodine vapor doping. Acid doping was further investigated to catalyze imine bond exchange and was found to promote backbone planarity, leading to enhanced crystallinity and conductivity. Density functional theory (DFT) calculations showed that protonation of imine bonds significantly enhances molecular planarity, consistent with experimental observations. Overall, this work shows that dynamic covalent bond exchange provides a useful strategy to enhance the structural and electronic properties of semiconducting polymers.

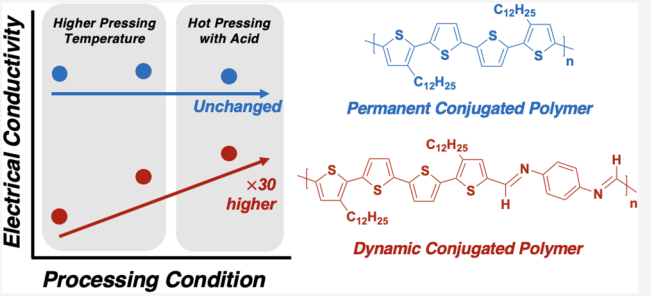

INTRODUCTION

Semiconducting polymers have received considerable attention due to their tunable optical, electrical, and mechanical properties for applications including organic field-effect transistors (OFETs),[1−5] organic photovoltaics (OPVs),[6−9] and sensors.[10−13] A common method for preparing conjugated polymer films relies on solution-processing, where polymers are dissolved into organic solvents followed by spin-coating,[14] drop-casting,[15] or blade-coating.[16] However, these methods require toxic solvents to dissolve conjugated polymers that are insoluble in more common organic liquids. Solid-state processing can produce films with thicknesses of a few microns[17] by heating above the melting temperature T_m to induce flow. However, many conjugated polymers exhibit high T_m values, and hot-pressing increases the risk of thermal oxidative degradation.[17] Stingelin and co-workers showed that hot-pressing can induce flow below T_m, successfully processing conjugated polymers into freestanding films.[18] Additionally, Deng and colleagues showed that hot-pressing below T_m enhanced the morphology and charge transport properties of poly(3,4-ethylenedioxythiophene) polystyrenesulfonate (PEDOT:PSS).[19] Scanning electron microscope (SEM) and X-ray diffraction (XRD) characterizations revealed that these improvements arise from continuous and tightly packed layered structures, with processed samples showing larger crystallites and reduced $\pi-\pi$ stacking distances.

Recently, the development of degradable or transient conjugated polymers has motivated a demand for sustainable, environmentally friendly, and self-healing electronic materials.[20] Imine-containing conjugated polymers are particularly promising due to their ease of synthesis and inherent degradability of the dynamic covalent bonds in acidic conditions.[20] Significant work has focused on understanding mechanisms of polymer degradability[20−22] rather than leveraging dynamic bond exchange to modulate crystallinity and conductivity. Prior work from our group showed that enhanced crystallinity is achieved via dynamic covalent bond exchange in nonconjugated oligoethylene networks with boronic ester cross-links, with crystallinity evolving slowly over 30 days at room temperature and ultimately reaching

Received: February 16, 2026
Revised: June 16, 2026
Accepted: July 20, 2026
Published: July 27, 2026

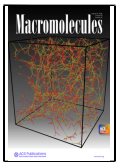

https://doi.org/10.1021/acs.macromol.6c00291
Macromolecules 2026, 59, 9015−9026

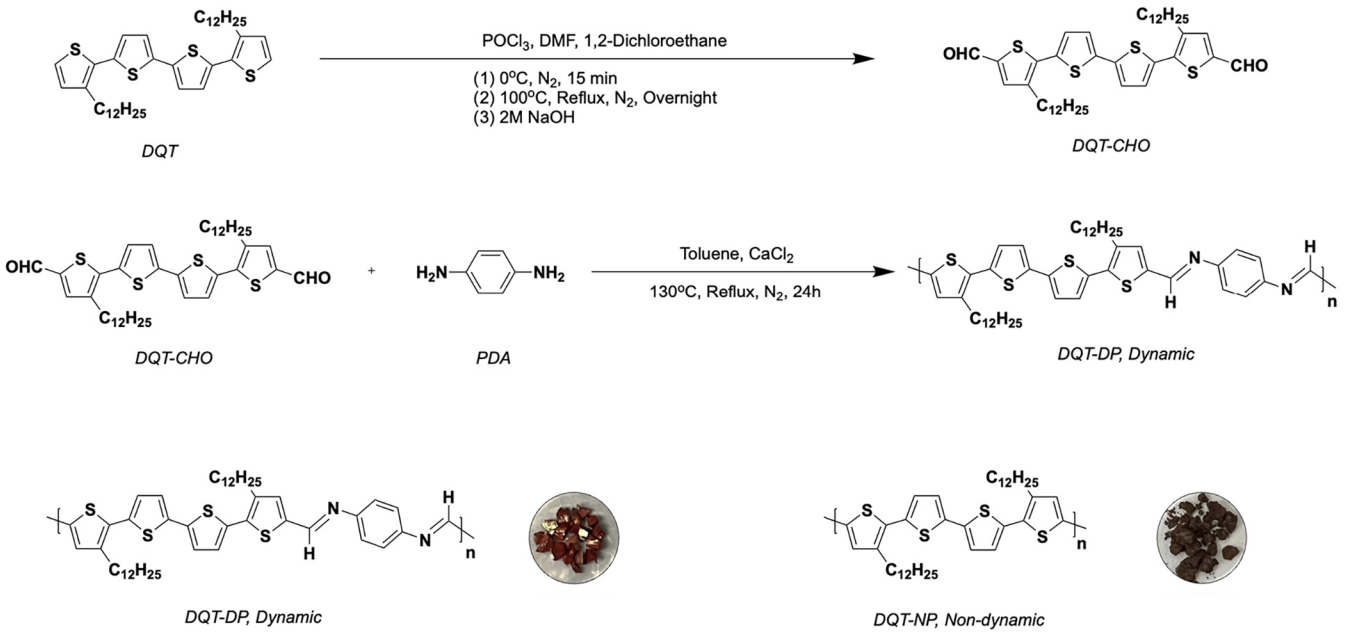

Figure 1. Synthesis and chemical structure of dynamic (DQT-DP) and nondynamic conjugated polymer (DQT-NP). DQT-CHO was obtained via Vilsmeier−Haack reaction. DQT-DP was synthesized by imine condensation of DQT-CHO with *p*-phenylene-diamine (PDA). DQT-NP was purchased commercially. The accompanying photographs show the neat polymers in their as-prepared states, without additional processing.

Table 1. Summary of Polymer Molecular Weight, Dispersity, and Thermal Transition

Polymer	M_n (kg/mol)	M_w (kg/mol)	$Đ$	DP[a]	T_g[b] (°C)	T_m[c] (°C)	T_d[d] (°C)
DQT-DP	16.5[e]/45.4[f]	95.7	5.8	21	53	237	380
DQT-NP	11.8	29.5	2.5	18	5[g]	49/66	420

[a]Degree of polymerization (DP) was calculated from M_n and M_w obtained by HT-GPC. (1,2,4-trichlorobenzene, 140 °C, relative to polystyrene standards). [b]Determined from the second heating DSC curves. [c]Determined from the first heating DSC curves. [d]Defined as the temperature at which the sample retained 95% of its initial mass, based on TGA data. [e]Estimated from ^{1}H NMR spectra of DQT-DP. [f]Measured by HT-GPC. [g]Glass transition overlapped with melting.

90%.[23] Elevated temperatures led to a crystal-crystal transition indicating the important role of bond exchanges on crystallinity. From this view, we posit that dynamic bond exchange in imine-linked conjugated polymers could similarly enhance crystallinity, thereby improving electrical conductivity compared to nondynamic conjugated polymers.

Dynamic covalent bond exchange is thermally activated and occurs with increased rates at elevated temperatures.[24] Acid catalysts can also accelerate imine exchange[26,27] and act as p-type dopants[28−31] in conjugated polymers. Therefore, both hot-pressing and acid doping are expected to govern imine bond exchange and crystallinity. Although imine-based conjugated polymers can degrade under acidic conditions, the degradation kinetics depend on the acid pK_a, polymer crystallinity, temperature, and acid concentration.[20,32−34]

In this work, we investigate how solid-state processing coupled with acid doping affects crystallinity and electron transport in dynamic conjugated polymers. Hot pressing temperature and differential scanning calorimetry (DSC) and wide-angle X-ray scattering (WAXS). Conductivity is enhanced by an order of magnitude after hot pressing at 170 °C and another order of magnitude with acid doping. In contrast, the nondynamic analogs show negligible changes in crystallinity or conductivity with similar processing. Overall, this work provides insights for designing facile processable conjugated polymers with dynamic covalent bonds as a route to enhance their performance.

RESULTS AND DISCUSSION

Synthesis and Characterization of Dynamic (DQT-DP) and Non-Dynamic (DQT-NP) Conjugated Polymers

3,3‴-Didodecyl-2,2′:5′,2″:5″,2‴-quaterthiophene (DQT) was end-functionalized with aldehyde groups through the Vilsmeier−Haack reaction, yielding DQT-CHO (Figure 1) and characterized using ^{1}H nuclear magnetic resonance (NMR) (Figure S1a). The dynamic conjugated polymer (DQT-DP) was synthesized via imine condensation from DQT-CHO and *p*-phenylene-diamine (PDA) (see Experimental Section). The nondynamic conjugated polymers (DQT-NP) were purchased from a commercial chemical vendor (Sigma-Aldrich).

In this work, no acid-catalyst was employed to form the imine bonds, in contrast to some previous studies where acid-catalysts were incorporated to achieve high molecular weight polymers.[11,12,24] Results from high-temperature gel permeation chromatography (HT-GPC) in trichlorobenzene indicated that the number-average molecular weight M_n of DQT-DP was 16 500 g/mol relative to polystyrene standards.[21,22,24] High dispersity samples ($Đ$ = 5.9) were obtained due to the inherent nature of polycondensation. Solution ^{1}H NMR spectra of DQT-DP displayed two characteristic peaks (Figure S1b), corresponding to imine bonds (HC = N, 8.3 ppm) and aldehyde end groups (CHO, 9.6 ppm), with an M_n value of 45 400 g/mol calculated from the ratio of the integrated peak areas in NMR spectra. Although the M_n value determined by

https://doi.org/10.1021/acs.macromol.6c00291
Macromolecules 2026, 59, 9015−9026

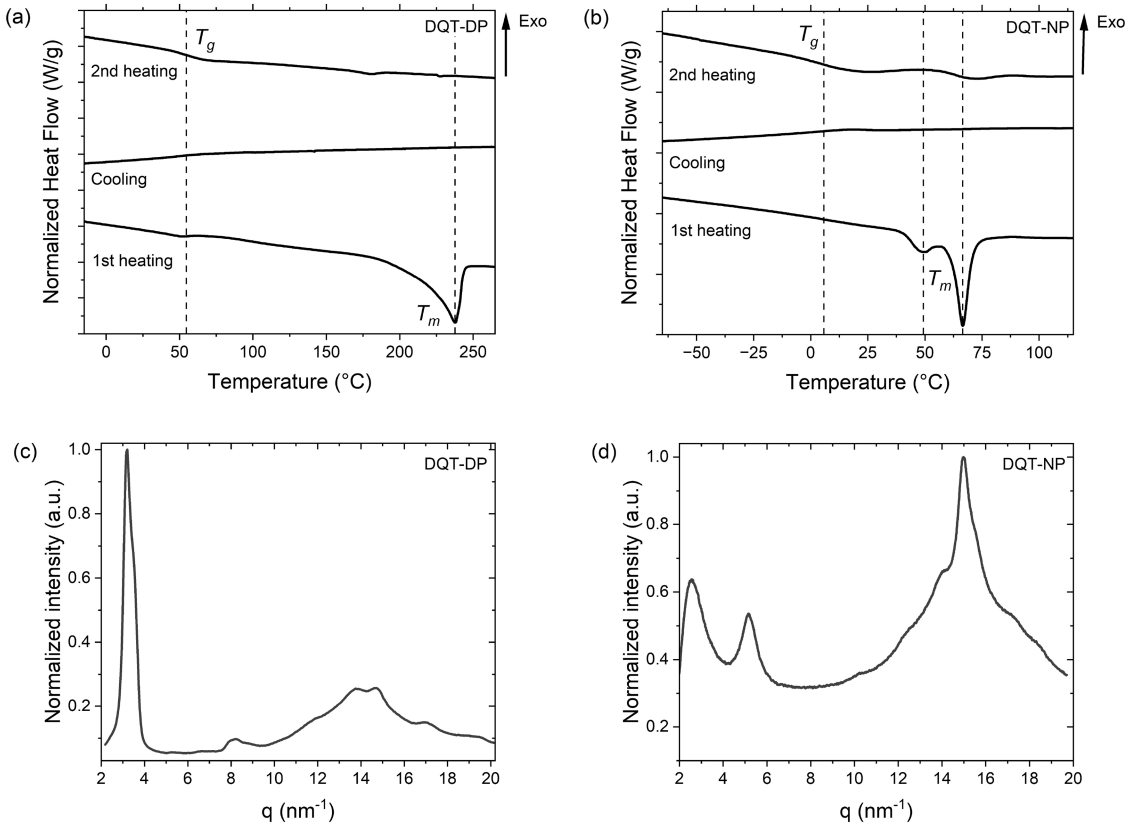

Figure 2. Thermal and X-ray scattering characterization of dynamic (DQT-DP) and nondynamic (DQT-NP) conjugated polymers. Differential scanning calorimetry (DSC) curves of neat (a) DQT-DP and (b) DQT-NP, recording at heating and cooling rate of 20 °C/min and 5 °C/min, respectively. Wide-angle X-ray scattering (WAXS) patterns of neat (c) DQT-DP and (d) DQT-NP.

NMR is higher than that measured by HT-GPC (Figure S2), NMR end-group analysis may be unreliable for high molecular-weight conjugated polymers due to limited sensitivity and additional limitations. In addition, we note that a high molecular weight DQT-DP was successfully obtained without acid catalyst based on its higher M_n relative to previously reported imine-based conjugated polymers prepared via acid-catalyzed polymerization.[21] In comparison, DQT-NP exhibited a lower M_n than DQT-DP (Table 1). Results from attenuated total reflectance Fourier transform infrared (ATR-FTIR) spectra and solid-state ^{13}C NMR are consistent with the formation of imine bonds in DQT-DP (Figures S3 and S4). The thermal stability of both polymers was evaluated by thermal gravimetric analysis (TGA) under N_2 environment. Both DQT-DP and DQT-NP showed high thermal stability, with degradation temperatures >350 °C, where the polymers retained 95% of their initial weights (Figure S5). These results are summarized in Table 1, which are comparable to other imine-based conjugated polymers in prior work.[35,36]

Thermal and X-ray Scattering Characterization of DQT-DP and DQT-NP

Differential scanning calorimetry (DSC) was performed to characterize the glass transition temperature T_g and melting temperature T_m of polymer samples (Figure 2). During the first heating scan, DQT-DP showed a single T_m at 237 °C, whereas DQT-NP exhibited two peaks at 49 and 66 °C (Figure 2a,2b). The two melting peaks in DQT-NP were attributed to the melting of alkyl side chains and $\pi-\pi$ stacked domains, consistent with prior work.[37] The T_g values were determined from second heating curves, where subsequent recrystallization was minimal and produced a clearer step. As expected, DQT-DP exhibited a higher T_g value (53 °C) than DQT-NP (5 °C). The higher T_g and T_m values of DQT-DP are attributed to a more rigid backbone resulting from imine linkages and aromatic benzene units. Both polymers did not exhibit characteristic T_m peaks during the second heating scans compared to the first heating curves, which reflects their slow crystallization kinetics.

Wide-angle X-ray scattering (WAXS) measurements were performed to analyze the crystallinity prior to additional processing (Figure 2c,2d). WAXS measurements for DQT-NP samples were performed using a quartz tube substrate with negligible background (Figure S6). Scattering peaks observed at 2.5 nm^{-1} and 5.2 nm^{-1} in DQT-NP correspond to lamellar periodicity (a00) of alkyl side chain spacing in the out-of-plane direction. A scattering peak at 14.9 nm^{-1} was assigned to the periodicity of the polymer backbone, (0b0) in the in-plane direction. Similarly, DQT-DP showed lamellar stacking peaks of side chains at 3.2 nm^{-1} and 8.1 nm^{-1}. Interestingly, DQT-DP displayed two $\pi-\pi$ stacking (010) peaks at 13.7 nm^{-1} and 14.6 nm^{-1}, suggesting two different $\pi-\pi$ stacking spacings. A similar feature was reported in random poly(3-hexylthiophene-thiophene) copolymers, attributed to two coexisting $\pi-\pi$ stacking modes due to its intermediate backbone regularity.[38] Although DQT-DP is not a copolymer, we attributed this observation to configurational isomerism arising from imine bonds connecting quaterthiophene and benzene units.

https://doi.org/10.1021/acs.macromol.6c00291
Macromolecules 2026, 59, 9015−9026

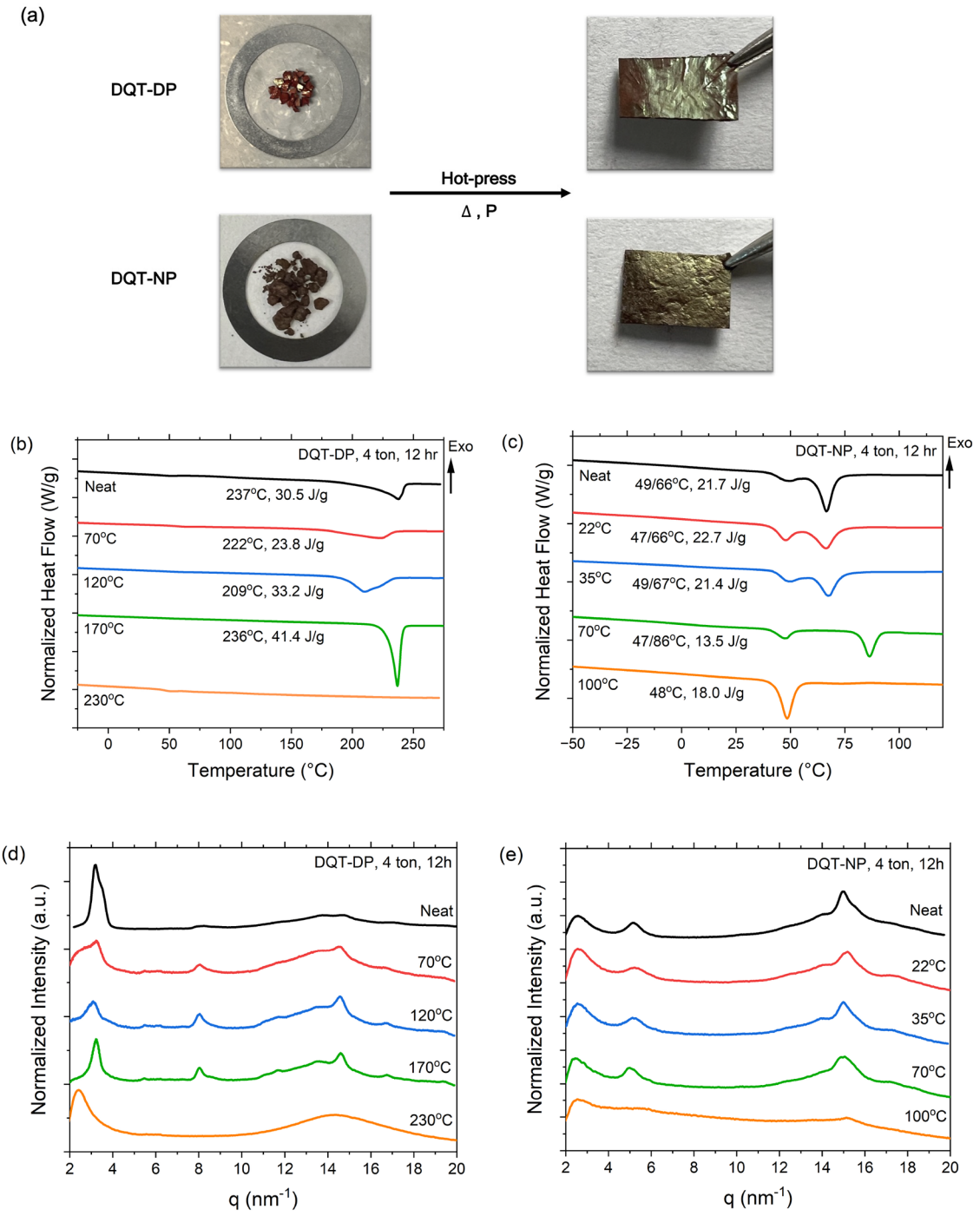

Figure 3. Solid-state processing of dynamic (DQT-DP) and permanent (DQT-PP) conjugated polymers via hot-pressing. (a) Illustrative scheme of solid-state processing. (b, c) Thermal and (d, e) morphological characterization of the polymers after solid-state processing via DSC and WAXS, respectively.

Enhanced Crystallinity and Electrical Conductivity in Dynamic Conjugated Polymer (DQT-DP) via Hot-Pressing Induced Dynamic Covalent Bond Exchange

Solution-phase processing of conjugated polymers generally requires sufficient solubility (>5 mg/mL) of polymers in organic solvents. We attempted to dissolve DQT-DP into various organic solvents including tetrahydrofuran, *N*,*N*-dimethylformamide, dimethyl sulfoxide, dichloromethane, and chloroform, but none of the solvents could dissolve DQT-DP at a concentration of at least 2 mg/mL with elevated temperatures (Figure S7). Among several chlorinated aromatic solvents including chlorobenzene, 1,2-dichlorobenzene, 1,2,4-trichlorobenzene, and 1-chloronaphthalene, only 1-chloronaphthalene successfully dissolved DQT-DP up to 10 mg/mL. Nevertheless, the high boiling point of this solvent (259 °C) complicates processing (e.g., spin coater with temperature control). Alternatively, solid-state processing methods preclude the use of potentially toxic organic solvents and the need for solvent evaporation.[39] Likewise, DQT-NP showed poor solubility in common organic solvents, but they were found to completely dissolve in chlorinated aromatic solvents. In this work, hot-pressing with controlled temperature and pressure

https://doi.org/10.1021/acs.macromol.6c00291
Macromolecules 2026, 59, 9015−9026

was used to produce freestanding micron-thick films (Figure 3a).

Prior work investigated imine bond exchange in small molecules in various solvents. The time scale for the exchange process of small molecules was a few minutes in deuterated solvents.[40] However, our polymers are prepared and characterized in the solid state, where the exchange rate is expected to be significantly slower due to restricted chain mobility. As a result, elevated temperatures are necessary to thermally activate and promote dynamic imine exchange.[23,24] Previous work demonstrated that imine bond exchange in the solid state can be activated above 100 °C with a time scale of several hours.[25] Similarly, dynamic imine exchange in DQT-DP is expected to occur during thermal annealing or hot-pressing under these conditions, enhancing crystallinity and charge transport, whereas DQT-NP is expected to be less affected by similar processing. All hot-pressed samples were quenched to room-temperature to kinetically trap the polymers. Processing temperature (above T_m, and three temperatures below T_m but above T_g), processing force (1−4 tons), and time (0.5−12 h) were varied systematically. First, the effect of temperature on crystallinity in DQT-DP was investigated by comparing T_m and the enthalpy of fusion (peak area). As the hot-pressing temperature increased, the T increased from 222 to 236 °C whereas the enthalpy increased from 30.5 J/g to 41.4 J/g (Figure 3b), indicating enhanced crystallinity.[41,42] The increase in the enthalpy of fusion is attributed to facilitated dynamic bond exchange promoted by higher thermal energy. Hot-pressing at 170 °C for 12 h did not significantly degrade the polymer as indicated by unchanged ATR-FTIR spectra (Figure S8). However, processing the sample at the melting transition at 230 °C resulted in severe thermal oxidative degradation. Thus, the hot-pressing duration at this temperature was limited to 2 h. Even with this relatively short processing time, no crystallinity was observed as indicated by the absence of a melting peak.

To understand the role of dynamic covalent bond exchange relative to flow-induced crystallinity, DQT-NP was processed below T_m and showed noticeable shifts in the two T_m peaks depending on temperature (Figure 3c). The higher T_m peak value increased but not the peak area. When the hot-pressing temperature exceeded T_m, only a single low temperature peak was observed. In this regime, cooling profiles significantly influence polymer morphology. Because all samples were rapidly quenched, DQT-NP showed reduced enthalpy compared to the neat polymer. Nevertheless, different pressing temperatures led to either more ordered domains (processing at 70 °C, higher T_m) or uniform domains (processing at 100 °C, single T_m).

WAXS experiments were further used to support the results from thermal characterization. As the hot-pressing temperature increased, the normalized intensity of $\pi-\pi$ stacking peaks in DQT-DP became stronger, indicating enhanced crystallinity resulting from faster imine bond exchange at elevated temperatures (Figure 3d). In contrast, the lamellar stacking peaks showed no clear trend either in peak width or normalized intensity, which is likely due to high sensitivity of low-q lamellar reflection on sample thickness and surface roughness.[43,44] As a result, the size and separation of crystallites associated with the side-chain morphology could not be quantitatively determined. On the other hand, $\pi-\pi$ stacking regions are less sensitive to these factors. The peak positions remained almost unchanged after processing, indicating that neither solid-state processing nor dynamic covalent bond exchange significantly altered the spacing between polymer chains. The selective enhancement of $\pi-\pi$ stacking peaks may arise from bond exchange occurring only along conjugated backbones. DQT-NP exhibited negligible variations in WAXS spectra under different hot-pressing conditions, attributed to the absence of dynamic covalent bonds (Figure 3e). Overall, these results show that increased hot-pressing temperatures enhance the crystallinity of DQT-DP samples, which is attributed to faster dynamic covalent bond exchange. Hot-pressing led to different distributions of crystallites in DQT-NP, but no increases in the enthalpy of melting. Additional processing parameters such as pressure and duration were also varied at a fixed temperature, but their effects on crystallinity were weaker compared to the influence of temperature (Figures S10 and S11). For example, DQT-DP was held at 170 °C in nitrogen for 12 h without applied pressure and the enthalpy increased from 30.6 J/g to 36.3 J/g indicating enhanced crystallinity; however, a processing force of 4 tons led to a higher enthalpy of 41.4 J/g (Figure S12). These results imply that pressure facilitates dynamic covalent bond exchange between polymer backbones by inducing flow. It is worth noting that only $\pi-\pi$ stacking peaks become more pronounced with sharper and higher normalized intensity WAXS peaks attributed to bond exchange primarily occurring along polymer backbones.

Enhanced $\pi-\pi$ stacking or increased crystallinity in conjugated polymers leads to improved electron transport, assuming that intermolecular electron hopping is the rate-limiting step rather than intramolecular transport along polymer backbones.[45] Due to the inherently low electrical conductivity of DQT-DP, iodine (I_2) vapor doping was applied to enhance electronic conductivity determined using four-point probe characterization (detailed procedures are described in the Experimental Section and Figure S13a). Iodine doping is a facile and effective method for doping for many p-type conjugated polymers.[46,47] Doping was visually confirmed by a color change to dark purple (Figure 4a). Electrical conductivity was measured in at least 3 different locations to account for heterogeneities in surface roughness and defects. The conductivity of DQT-DP at room temperature was comparable to a prior study with selenophene-based polyimines using an identical doping method.[48] As the hot-pressing temperature increased from room temperature to 170 °C, the conductivity of DQT-DP improved by more than an order of magnitude (Figure 4b), which is attributed to the improved crystallinity through dynamic bond exchanges, supported by DSC and WAXS results. In contrast, DQT-NP did not show conductivity improvements unless processed above T_m (Table 2). It should be noted that the intrinsic electrical conductivity of DQT-DP is 7−8 orders of magnitude less conductive than DQT-NP, which is likely due to the loss of heteroaromatic structure and the presence of configurational isomers.[49,50] Given this low electronic conductivity of DQT-DP, these polymers, as prepared, should not be viewed as direct substitutes for DQT-NP in applications requiring high electronic conductivity. Although introducing imine linkages into conjugated polymers leads to a diminished electrical conductivity, dynamic covalent bond exchange plays an important role in enhancing morphology and improving charge transport with sub-T_m processing, strategies that can be leveraged in future applications. In prior work, imine and vinyl linkages were introduced into the same conjugated

https://doi.org/10.1021/acs.macromol.6c00291
Macromolecules 2026, 59, 9015−9026

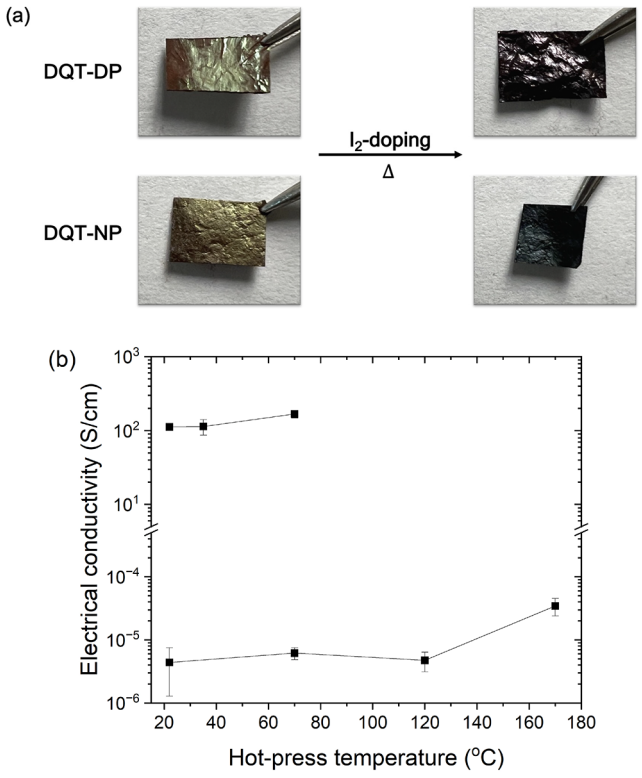

Figure 4. (a) Photos before and after iodine (I_2) vapor doping of dynamic (DQT-DP) and nondynamic (DQT-NP) conjugated polymers. The color of the samples changed from brown to dark purple, confirming successful iodine doping. (b) Electrical conductivity of dynamic conjugated polymers (DQT-DP) as a function of hot-pressing temperatures.

backbones. Although the hole mobility of imine polymers was lower than vinyl polymers, the difference was a factor of 5 rather than several orders of magnitude.[49] This comparison suggests that the severe conductivity loss observed in DQT-DP is not necessarily intrinsic to all imine-linked conjugated polymers but instead depends strongly on backbone design and structure. Therefore, future efforts could focus on imine-containing structures that preserve backbone planarity, suppress linkage disorder, and maintain stronger electronic coupling. Beyond these considerations, mixed ionic/electronic conduction may provide an alternative strategy for mitigating the drawbacks associated with reduced electronic conductivity of dynamic polymer (DQT-DP). Recent studies have reported the successful synthesis of imine-based conjugated polymers where ionic contributions can promote charge compensation and enhance hole mobility compared to related materials lacking ionic transport.[55,56]

Improved Crystallinity and Electrical Conductivity in Dynamic Conjugated Polymers (DQT-DP) via Acid-Catalyzed Imine Bond Exchange and Protonation-Induced Planarity

To determine whether improved crystallinity and electrical conductivity of DQT-DP originate from dynamic bond exchange or from flow-induced chain alignment, acid doping was used to accelerate bond exchange kinetics. Protons catalyze imine exchange by reducing the activation energy[26,27] and function as p-type dopants by protonating conjugated polymer backbones.[28−31] Imine bonds can also be protonated depending on the acid concentration.[32] Although imine-based conjugated polymers may degrade under acidic conditions, the degradation kinetics depend on acid pK_a, polymer morphology, temperature, and acid concentration.[20,32,33] Here, *p*-toluene sulfonic acid (PTSA) was selected for acid-doping (Experimental Section, Figures 5a and S13b). To minimize polymer degradation, ethanol was chosen as the solvent due to its limited solubility for conjugated polymers. After acid doping, a new peak at 1635 cm^{-1} emerged, and the peak at 1593 cm^{-1} shifted to 1580 cm^{-1} in ATR-FTIR spectra (Figure 5b), similar to prior reports.[32,33,51] In addition, acid treated DQT-DP did not show an aldehyde peak which would result from potential degradation to DQT-CHO. These results suggest that protonation of imine bonds occurred without significant polymer degradation. The chemical structures of DQT-DP upon acid doping and protonation are shown in Figure 5c.

The effect of protonated imine bonds on crystallinity was analyzed using DSC and WAXS. Protonation resulted in higher T_m compared to pristine samples, but the corresponding enthalpy of fusion decreased with increased acid concentration (Figure 6a). This observation indicates the formation of fewer, yet more ordered crystallites, as reported previously.[52] WAXS patterns show that the intensity ratio between peaks at 13.5 nm^{-1} and 14.5 nm^{-1} changed with increasing acid concentrations (Figure 6b). The relative intensity of the peak at 13.5 nm^{-1} gradually increased, eventually becoming similar to the peak at 14.5 nm^{-1}, which likely occurs due to acid-catalyzed isomerization of trans−trans to cis−cis isomers. The trans−trans isomers are thermodynamically favored and dominant in

Table 2. Electrical Conductivity of Dynamic (DQT-DP) and Non-Dynamic (DQT-NP) Conjugated Polymers, Measured by Four-Point Probes at Room Temperatures[a]

Hot-pressing temperature[b]	22 °C	70 °C	120 °C	170 °C
DQT-DP[c]	$4.4 \times 10^{-6} \pm 3.12 \times 10^{-6}$ S/cm	$8.5 \times 10^{-6} \pm 6.18 \times 10^{-6}$ S/cm	$4.7 \times 10^{-6} \pm 1.62 \times 10^{-6}$ S/cm	$3.5 \times 10^{-5} \pm 1.06 \times 10^{-5}$ S/cm
Acid concentration[d]	0 w/v%	1 w/v%	2.5 w/v%	5 w/v%
DQT-DP[e]	$1.2 \times 10^{-5} \pm 1.89 \times 10^{-5}$ S/cm	$6.2 \times 10^{-5} \pm 1.26 \times 10^{-5}$ S/cm	$3.6 \times 10^{-5} \pm 7.12 \times 10^{-6}$ S/cm	$1.4 \times 10^{-4} \pm 2.98 \times 10^{-5}$ S/cm

Hot-pressing temperature[b]	22 °C	35 °C	70 °C
DQT-NP[c]	112 ± 10.1 S/cm	114 ± 27.1 S/cm	168 ± 20.6 S/cm
Acid concentration[d]	0 w/v%		5 w/v%
DQT-NP[e]	128 ± 14.6 S/cm		119 ± 12.9 S/cm

[a]Three different locations were measured and obtained values were averaged to reflect the surface roughness and defects of the samples [b]Parameters including pressing force and duration were fixed at 4 tons and 12 h. [c]Four-point probes measurements were performed after I_2 vapor doping. [d]*p*-toluenesulfonic acid (PTSA) was used for acid doping. [e]Acid doping was followed by the subsequent I_2 vapor doping. The conductivity of the iodine-doped samples decreased upon aging due to iodine sublimation.

https://doi.org/10.1021/acs.macromol.6c00291
Macromolecules 2026, 59, 9015−9026

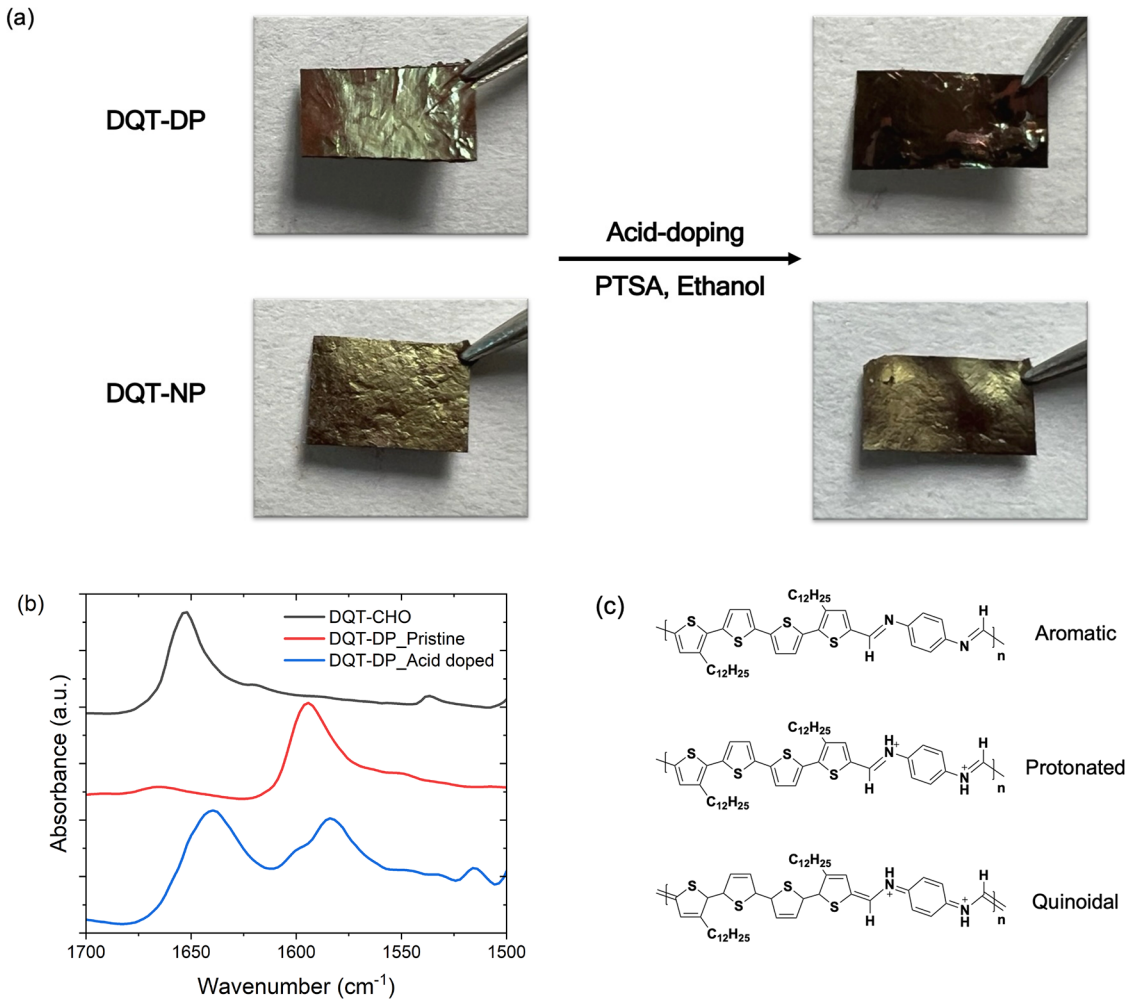

Figure 5. (a) Photos before and after acid doping of dynamic (DQT-DP) and nondynamic (DQT-NP) conjugated polymers. (b) ATR-FTIR spectra of monomer (DQT-CHO), pristine, and acid-doped DQT-DP, confirming the successful protonation of imine bonds without significant degradation. (c) Neutral aromatic, acid-protonated, and quinoidal resonance structures for DQT-DP, leading to more planar structures.

the pristine undoped sample, but acid can alter the equilibrium between cis and trans isomers. McAllister and colleagues investigated acid-catalyzed Z/E isomerization in imine compounds, and results from this prior study are consistent with this interpretation.[53]

Acid doping did not significantly affect lamellar structures derived from side chains because imine bonds are confined to the conjugated backbones. A series of experiments was performed with hot pressing before or after acid doping, as well as acid doping with thermal annealing and no pressure, followed by DSC and WAXS analysis (Figure 6c,d). We hypothesized that hot-pressing after acid doping would lead to a large enhancement in crystallinity due to accelerated bond exchange. Indeed, only the polymer sample subjected to hot-pressing after acid doping exhibited changes in the ratio of two $\pi-\pi$ stacking intensities, suggesting that these changes arise mainly from imine bond exchange rather than acid doping alone (Figure 6d). However, a peak at 17.7 nm^{-1} appeared regardless of the processing sequence, indicating protonated imine bonds promote closer $\pi-\pi$ spacing due to enhanced backbone planarity.[45] As expected, acid doping had no significant effect on the morphology of DQT-NP before and after acid doping (Figure S13).

Enhanced $\pi-\pi$ interactions are expected to improve electrical conductivity. The electrical conductivity of DQT-DP samples doped with acid was measured after subsequent I_2 vapor doping (Figure 7). Notably, the DQT-DP sample with the largest acid doping exhibited nearly an order of magnitude higher conductivity compared to the pristine sample due to its enhanced crystallinity arising from protonation-induced planarity and acid-catalyzed imine bond exchange. In contrast, the electrical conductivity of DQT-NP remains unchanged after acid doping and I_2 vapor doping (Table 2), supported by no significant differences in DSC and WAXS spectra.

DFT Simulations of Protonation-Induced Planarity and $\pi-\pi$ Stacking in DQT-DP Isomers

Density functional theory (DFT) calculations were performed to elucidate the effect of protonation on the DQT-DP backbones, using methods consistent with prior literature.[32] Six representative model compounds corresponding to the cis−cis, cis−trans, and trans−trans conformers of DQT-DP in both neutral and protonated forms were fully optimized (Figure 8). For computational simplicity, dodecyl alkyl chains were replaced with methyl groups. Geometry optimizations were carried out using the ωB97x-3c composite method, and implicit solvation was modeled using the conductor-like polarizable continuum model (CPCM) with a dielectric

https://doi.org/10.1021/acs.macromol.6c00291
Macromolecules 2026, 59, 9015−9026

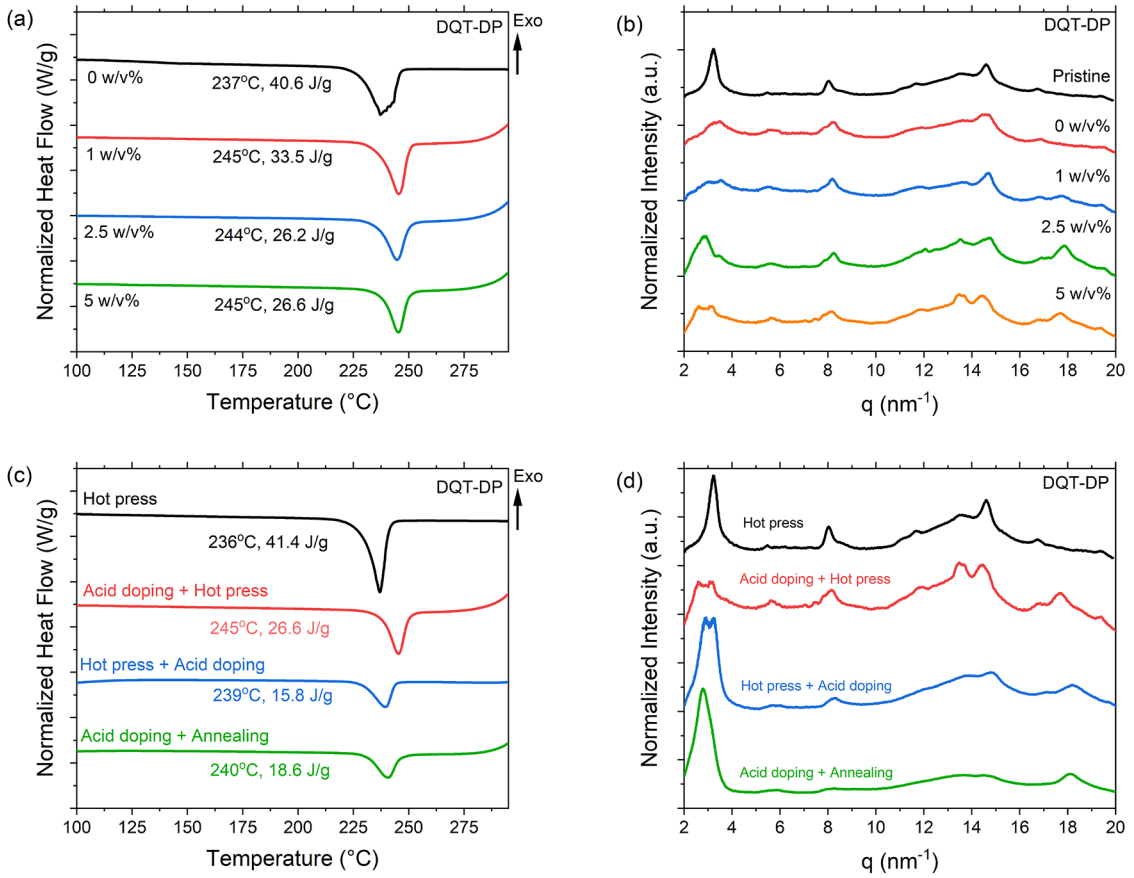

Figure 6. Effect of acid doping and hot press on thermal, morphological, and electrical properties of dynamic conjugated polymers (DQT-DP). (a) DSC curves and (b) WAXS patterns as a function of *p*-toluene sulfonic acid (PTSA) concentration. 0 w/v% is a control sample where no acid was introduced, but processed with identical doping procedures. (c) DSC curves and (d) WAXS patterns with various combinations of processes.

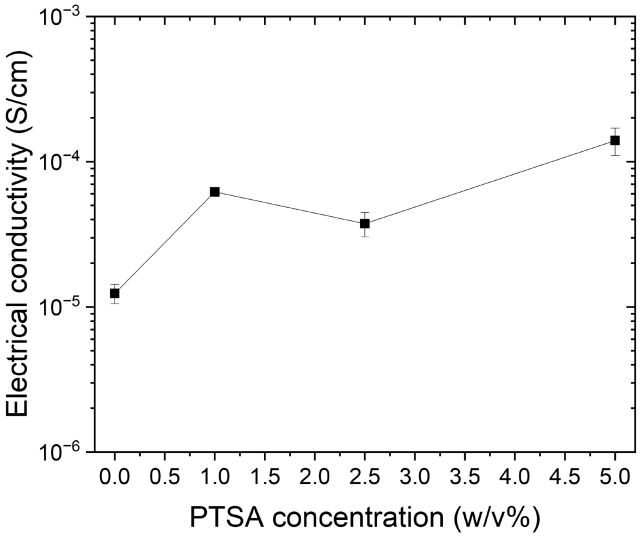

Figure 7. Electrical conductivity of dynamic conjugated polymers (DQT-DP) as a function of p-toluene sulfonic acid (PTSA) concentration, followed by I_2 vapor doping. The conductivity increased an order of magnitude higher than the control sample where no acid dopant was introduced.

constant (ε = 4) to approximate the effects of neighboring polymer molecules (Figure S15).

Bond-length alternation (BLA) was calculated as the difference between the average lengths of single and double bonds along the conjugated backbone for all DQT-DP structures. Taking the trans−trans conformer as an example, the BLA decreases from 0.073 Å in the neutral state to 0.049 Å upon protonation, indicating a more quinoidal backbone. The increased quinoidal character upon protonation promotes greater backbone rigidity and planarity, consistent with increased double-bond character in the linker C−C bonds connecting the aromatic rings. When the analysis is restricted to the benzene, imine, and the innermost thiophene units—excluding the outer thiophenes due to their weak electronic coupling to the imine—the decrease in BLA is more pronounced, from 0.069 Å in the neutral state to 0.023 Å upon protonation. Similar decreases in BLA upon protonation are observed for the cis−cis and cis−trans conformers (Figure S16).

To quantify molecular coplanarity, the plane of best fit (PBF) was calculated for each structure, where smaller PBF values correspond to more planar geometries (PBF ∼ 0 for highly planar structures, ∼0.2−1.0 for moderately distorted backbones, and >1.0 for strongly nonplanar conformations).[54] To estimate robust statistical ensembles and associated uncertainties, conformational ensembles were generated from the DFT-optimized geometries of each compound using Open Babel (∼50 conformers per configuration) via MMFF94-based DiverseConfGen conformer generation (energy window = 1000 kcal mol^{-1}; RMSD cutoff during generation = 0.1 Å), and only structures within a prescribed RMSD-to-reference threshold (RMSD < 3 Å after alignment to the DFT minimum) were

https://doi.org/10.1021/acs.macromol.6c00291
Macromolecules 2026, 59, 9015−9026

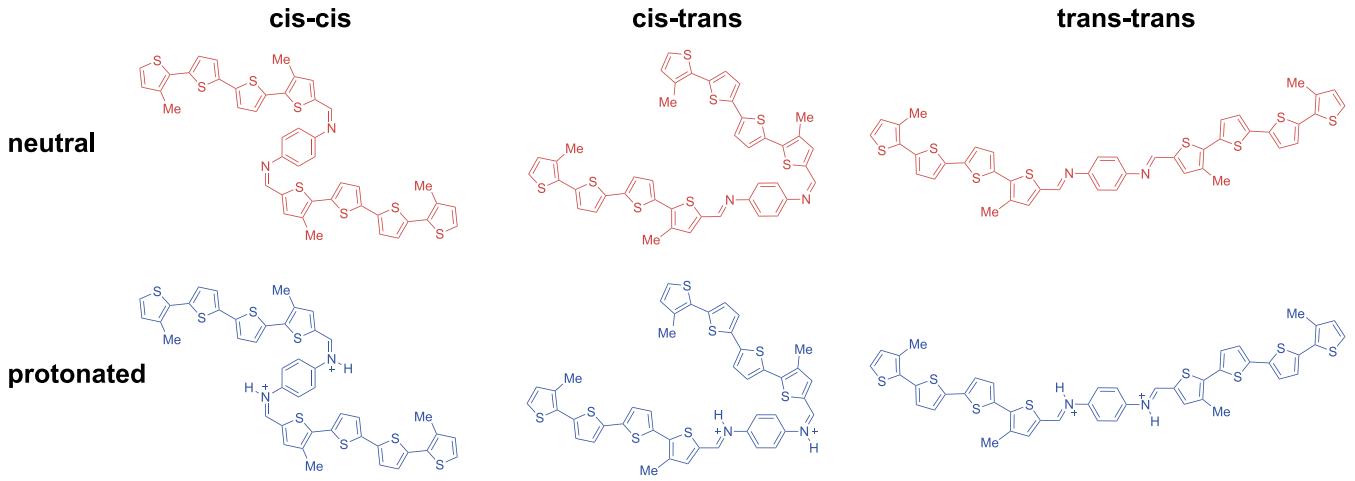

Figure 8. Model compounds representing the neutral and protonated polymers as cis−cis, cis−trans, and trans−trans conformers.

retained to sample local distortions around the optimized minimum; each retained conformer was then optimized with GFN2-xTB, and the resulting geometries were used to compute PBF.

For the trans−trans configuration, the PBF value decreases from 0.75 ± 0.33 in the neutral state to 0.24 ± 0.13 upon protonation, indicating that protonation significantly enhances backbone coplanarity (Table 3). Similarly, the PBF for the cis−cis configuration decreased from 0.70 ± 0.23 in the neutral state to 0.60 ± 0.29 after protonation. The substantially lower PBF value of the protonated trans−trans conformer (0.24 ± 0.13) compared to the protonated cis−cis conformer (0.60 ± 0.29) indicates that protonation preferentially stabilizes a planar backbone in the trans−trans configuration, while the cis−cis configuration remains significantly more distorted.

Table 3. Plane of Best Fit (PBF) Values for Neutral and Protonated Forms of cis−cis, cis-trans, and trans−trans Conformers of DQT-DP Model Compounds

Isomer	State	Plane of Best Fit (PBF)
cis−cis	Neutral	0.70 ± 0.23
	Protonated	0.60 ± 0.29
cis−trans	Neutral	0.86 ± 0.24
	Protonated	0.81 ± 0.11
trans−trans	Neutral	0.75 ± 0.33
	Protonated	0.24 ± 0.13

In addition to PBF values, dihedral angles between the (hetero)aryl rings and the imine linkages were calculated for each structure (Figure S17 and Table S1). Across all conformers, protonation leads to an average increase in the dihedral angles of approximately 6°, indicating a modest increase in backbone planarity. Notably, for the dihedral angle between the imine linkage and the benzene ring, the cis imine bond exhibits a value of 93.9°, whereas the trans imine bond displays a substantially larger dihedral angle of 148.2°, further supporting that the trans−trans conformer adopts a more planar backbone geometry than the cis−cis conformer.

Overall, the computational results demonstrate that protonation induces a pronounced decrease in bond-length alternation, directly indicating stabilization of a more quinoidal, rigid, and planar DQT-DP backbone. This protonation-induced increase in planarity is supported by decreased PBF values and increased inter-ring dihedral angles across all conformers and is consistent with the emergence of the $\pi-\pi$ stacking peak at 17.7 nm^{-1} in the WAXS patterns upon PTSA treatment. (Figure 6b), reflecting closer intermolecular packing enabled by protonation. A more detailed understanding of the $\pi-\pi$ stacking features at 13.5 and 14.5 nm^{-1} in the WAXS patterns will require future molecular dynamics simulations to directly estimate intermolecular $\pi-\pi$ stacking distances for the cis−cis and trans−trans conformations.

CONCLUSIONS

In this work, we show that solid-state processing combined with acid doping significantly improves crystallinity and electrical conductivity of dynamic imine-based conjugated polymers (DQT-DP) relative to nondynamic analogues (DQT-NP). Hot-pressing of DQT-DP below its melting point T_m effectively facilitates dynamic imine bond exchanges, resulting in increased melting peak enthalpy and tighter $\pi-\pi$ stacking as the pressing temperature increased. The electrical conductivity of DQT-DP, after iodine (I_2) vapor doping, increased up to ~10^{-5} S/cm, which is attributed to morphological improvement. Acid doping using p-toluene sulfonic acid (PTSA) further promoted polymer planarity and crystallinity via proton-catalyzed exchange, leading to another order of magnitude enhancement in electrical conductivity (~10^{-4} S/cm) upon subsequent I_2 vapor doping. In contrast, the nondynamic polymer DQT-NP exhibited minimal morphological or conductivity changes after hot-pressing and acid doping. Results from density functional theory (DFT) simulations showed that protonation of imine bonds substantially increased backbone planarity, which supports our experimental observations of enhanced $\pi-\pi$ stacking and conductivity. Overall, our results suggest that leveraging dynamic covalent bond exchanges through controlled solid-state processing and acid doping offers a versatile route to tailor morphology and charge transport properties in conjugated polymers.

EXPERIMENTAL SECTION

Materials

3,3‴-didodecyl-2,2′:5′,2″:5″,2‴-quarterthiophene (DQT, 95%) was purchased from Ambeed. *p*-phenylene-diamine (PDA, 99+%), anhydrous toluene (≥99.8%, DriSolv), hexane (HPLC grade), and

https://doi.org/10.1021/acs.macromol.6c00291
Macromolecules 2026, 59, 9015−9026

dichloromethane (DCM, ACS reagent) were obtained from Fisher Scientific. Anhydrous sodium sulfate (Na_2SO_4, ≥99%) was purchased from Thermo Scientific. PQT-12 (DQT-NP), p-toluene sulfonic acid monohydrate (ACS regent, 98.5%), anhydrous ethyl alcohol (≥99.5%), iodine flakes (≥99%), and anhydrous 1,2-dichloroethane (99.8%) were purchased from Sigma-Aldrich. Phosphorus(V) oxychloride was obtained from Oakwood Chemical, and 1,2,4-trichlorobenzene-d_3 (98%) from 10X Chem LLC. Methanol (ACS grade), sodium hydroxide (NaOH, ACS grade), sodium chloride (NaCl, ACS grade), and anhydrous calcium chloride (ACS grade) were purchased from VWR Chemicals. Anhydrous *N*,*N*-dimethylformamide (DMF) was prepared from a solvent purification system. All chemicals were used as received without further purification.

Synthetic Procedures

Functionalization of DQT (DQT-CHO). To prepare a Vilsmeier reagent, anhydrous DMF (10 equiv, 15 mmol) was added into an oven-dried 100 mL round-bottom flask containing a stir bar, and the mixture was cooled to 0 °C. $POCl_3$ (10 equiv, 15 mmol) was then added dropwise at 0 °C, and the reaction mixture was stirred for 15 min. In a separate flask, QTH (1 equiv, 1.5 mmol) was prepared followed by the addition of anhydrous 1,2-dichloroethane. Then, the reaction solution was vigorously mixed until complete dissolution. The freshly prepared Vilsmeier reagent was transferred into the QTH/1,2-dichloroethane mixture by dropwise addition at room temperature. After stirring for 15 min, the reaction mixture was refluxed overnight at 100 °C. All procedures were conducted under a nitrogen atmosphere unless otherwise noted. The reaction was quenched with 2 M NaOH and extracted with DCM and brine. The collected organic layer was dried over Na_2SO_4 and filtered. The crude product was purified using an automated flash chromatography system (Biotage) with a 9:1 mixture of DCM and hexane.

^{1}H NMR (500 MHz, dichloromethane-d_2): δ9.76 (s, 2H), δ7.54 (s, 2H), δ7.24 (m, 4H), δ2.77 (m, 4H), δ1.62 (m, 4H), δ1.31 (m, 36H), δ0.80 (t, 6H)

Dynamic Conjugated Polymers (DQT-DP) Synthesis. The prepared DQT-CHO (1 equiv, 1.38 mmol) was added to an oven-dried round-bottom flask with a stir bar. Then, PDA (1 equiv, 1.38 mmol) and anhydrous toluene were added. The mixture was vigorously stirred at 70 °C under ambient air conditions until complete dissolution. Oven-dried $CaCl_2$ (150 mg) was introduced as a drying agent. The reaction mixture was then refluxed at 130 °C for 24 h under a nitrogen atmosphere. Upon completion, the flask was removed from the oil bath and allowed to cool to room temperature. The resulting mixture was concentrated using a rotary evaporator and further dried under vacuum at 130 °C overnight. Red solids were obtained as the final products without further purification.

ATR-FTIR. A Bruker α FT-IR spectrometer with a platinum-ATR QuickSnap sampling module was used to obtain infrared spectra. The scanning range was from 4000 cm^{-1} to 400 cm^{-1} with 32 scans and 4 cm^{-1} resolution.

Solution-Phase NMR. A Carver B500 Bruker Advance III HD (500 MHz) NMR spectrometer with BBFO CryoProbe was used to obtain ^{1}H spectra. Monomers were dissolved in DCM-d_2 under ambient conditions. The polymer sample was dissolved in 1,2,4-trichlorobenzene-d_3 by heating 140 °C overnight in an argon-filled glovebox.

Solid-State NMR. A Carver Bruker 500WB (500 MHz) NMR spectrometer with Phoenix HXY MAS probe was used to obtain ^{13}C spectra at 25 and 100 °C. The sample was packed into a 6 mm rotor inside an argon glovebox. Adamantane was used as the external ^{13}C chemical shift reference.

Differential Scanning Calorimetry (DSC). DSC curves were taken on a TA Instruments DSC 2500. Samples were prepared in Tzero aluminum pans and subjected to a heat/cool/heat cycle in a temperature range from −100 to 100 °C at 20 °C/min for heating and 5 °C/min for cooling for all samples.

Thermogravimetric Analysis (TGA). The thermal stability of the polymer samples was characterized by a TA Instruments Q50. Each sample was heated at a rate of 10 °C/min under N_2 from 30 to 600 °C.

High Temperature-Gel Permeation Chromatography (HT-GPC). Number-average molecular weight (M_n), weight-average molecular weight (M_w), and dispersity ($Đ$) for dynamic conjugated polymers (DQT-DP) were characterized by high temperature-gel permeation chromatography (HT-GPC) on Toshoh EcoSEC (model) with a refractive index detector. HPLC (high-performance liquid chromatography) grade 1,2,4-trichlorobenzene containing 500 ppm BHT (butylated hydroxytoluene) stabilizer was used as the eluent at 140 °C with a flow rate of 0.6 mL/min. The system was calibrated with polystyrene standards. All samples were prepared with a concentration of 2 mg/mL using the same solvent. The samples were stirred for 2 h at 140 °C before loading on the instrument.

Solid-State Processing (Hot Press). Each polymer was placed between two stainless steel plates and pressed at 22, 35, 45, 70, 130, 170, or 230 °C for 0.5, 2, or 12 h under 1, 2, or 4 tons pressure, depending on their thermal transition temperatures (T_g and T_m). The resulting film thickness ranged from 20 to 300 μm, depending on the processing conditions.

Wide-Angle X-ray Scattering (WAXS). The crystallinity of polymers was examined using a Xenocs GeniX3D Cu Kα X-ray source (1.54 Å) with a Pilatus 2D detector. A road beam stop is located in front of the detector to dampen the primary beam. A silver behenate powder was used to calibrate the sample-to-detector distance. Raw samples were packed in a 1 mm thick quartz capillary tube and sealed with marine epoxy (Devcon, home 5 min Epoxy) for ease of sample loading. All measurements were conducted under ambient conditions with a 30 min exposure time. FIT2D software was used to process2D diffraction data into plots of intensity versus scattering vector.

Iodine Vapor Doping. Iodine flakes were weighed and added to a 2 mL vial. The vial was inserted into a 20 mL vial, which was heated at 70 °C for 15 min in an oven. Each polymer sample, prepared using the solid-state processing method, was promptly added, resealed, and returned to the preheated oven at 70 °C. After 2 h, the vial was removed and allowed to cool to room temperature.

Acid Doping. Acid doping solutions (0, 1, 2.5, and 5 w/v%) were prepared by dissolving *p*-toluene sulfonic acid (PTSA) into 2 mL of anhydrous ethanol. Each polymer sample was fully immersed in the solution. After 12 h, the sample was removed, washed with ethanol, and subsequently dried under a nitrogen flow at room temperature for another 12 h.

Electrical Conductivity Measurements (Four-Point Probes). Electrical conductivity was measured using a Jandel 4-point probe system (RM3-AR) at room temperature under ambient conditions. The electrode spacing was 1.59 mm. Three different points on both the front and back sides of each sample were measured to reflect rough surface morphology after solid-state processing.

Computational Details—Density Functional Theory (DFT) Simulations. Geometry optimizations were performed using density functional theory (DFT) with the Orca software suite using the following composite functional and solvent model: wB97x-3c CPCM(ε = 4). Conformational ensembles were generated from the DFT-optimized geometries using Open Babel's Confab search (~50 conformers per configuration each within 3 Å root mean squared distance from the DFT optimized geometry), sampling local distortions around the optimized minimum. Each conformer was subsequently optimized using the GFN2-xTB ALPB(ε = 4).

■ ASSOCIATED CONTENT

Supporting Information

The Supporting Information is available free of charge at https://pubs.acs.org/doi/10.1021/acs.macromol.6c00291.

High-temperature GPC results of dynamic (DQT-DP) and permanent (DQT-NP) conjugated polymers; thermal gravimetric analysis (TGA) curves of dynamic (DQT-DP) and non-dynamic (DQT-NP) conjugated

https://doi.org/10.1021/acs.macromol.6c00291
Macromolecules 2026, 59, 9015−9026

polymers, and dihedral angles between the (hetero)aryl rings and the imine linkages for each structure (PDF)

AUTHOR INFORMATION

Corresponding Authors

Charles M. Schroeder − *Department of Materials Science and Engineering, Materials Research Laboratory, Beckman Institute for Advanced Science and Technology, and Department of Chemical and Biomolecular Engineering, University of Illinois Urbana—Champaign, Urbana, Illinois 61801, United States;* Present Address: Department of Chemical and Biological Engineering, Princeton University, 41 Olden Street, Princeton, New Jersey 08544, United States; orcid.org/0000-0001-6023-2274; Email: cschroeder@princeton.edu

Christopher M. Evans − *Department of Materials Science and Engineering, Materials Research Laboratory, and Department of Chemical and Biomolecular Engineering, University of Illinois Urbana—Champaign, Urbana, Illinois 61801, United States;* orcid.org/0000-0003-0668-2500; Email: cme365@illinois.edu

Authors

Seongon Jang − *Department of Materials Science and Engineering, Materials Research Laboratory, and Beckman Institute for Advanced Science and Technology, University of Illinois Urbana—Champaign, Urbana, Illinois 61801, United States*

Jason L. Wu − *Beckman Institute for Advanced Science and Technology and Department of Chemistry, University of Illinois Urbana—Champaign, Urbana, Illinois 61801, United States*

Nicholas E. Jackson − *Beckman Institute for Advanced Science and Technology and Department of Chemistry, University of Illinois Urbana—Champaign, Urbana, Illinois 61801, United States;* orcid.org/0000-0002-1470-1903

Complete contact information is available at: https://pubs.acs.org/10.1021/acs.macromol.6c00291

Notes

The authors declare no competing financial interest.

ACKNOWLEDGMENTS

The authors gratefully acknowledge the use of research facilities at Material Research Laboratory, Beckman Institute for Advanced Science and Technology, and School of Chemical Sciences NMR Laboratory at the University of Illinois Urbana−Champaign. The authors acknowledge Dr. Alex Balzer and Prof. Thomas H. Epps, III at University of Delaware for conducting HT-GPC sample measurements. This project was supported by the Army Research Office, Polymer Chemistry Program (grant W911NF-24-1-0248, dynamic crystalline materials) and the National Science Foundation (NSF) via the Molecular Maker Lab Institute (Award 201987, NSF AI Institute, molecular design).

REFERENCES

(1) Dimitrakopoulos, C. D.; Malenfant, P. R. L. Organic Thin-Film Transistors for Large-Area Electronics. *Adv. Mater.* **2002**, *14* (2), 99−117.

(2) Yang, J.; Zhao, Z.; Wang, S.; Guo, Y.; Liu, Y. Insight into High-Performance Conjugated Polymers for Organic Field-Effect Transistors. *Chem* **2018**, *4* (12), 2748−2785.

(3) Kim, M.; Ryu, S. U.; Park, S. A.; Choi, K.; Kim, T.; Chung, D.; Park, T. Donor-Acceptor-Conjugated Polymer for High-Performance Organic Field-Effect Transistors: A Progress Report. *Adv. Funct. Mater.* **2020**, *30* (20), No. 1904545.

(4) Ashizawa, M.; Zheng, Y.; Trans, H.; Bao, Z. Intrinsically stretchable conjugated polymer semiconductors in field effect transistors. *Prog. Polym. Sci.* **2020**, *100*, No. 101181.

(5) Lei, T.; Cao, Y.; Fan, Y.; Liu, C.-J.; Yuan, S.-C.; Pei, J. High-Performance Air-Stable Organic Field-Effect Transistors: Isoindigo-Based Conjugated Polymers. *J. Am. Chem. Soc.* **2011**, *133* (16), 6099−6101.

(6) Sariciftci, N. S.; Smilowitz, L.; Heeger, A. J.; Wudl, F. Photoinduced Electron Transfer from a Conducting Polymer to Buckminsterfullerene. *Science* **1992**, *258* (5087), 1474−1476.

(7) Coakley, K. M.; McGehee, M. D. Conjugated Polymer Photovoltaic Cells. *Chem. Mater.* **2004**, *16* (23), 4533−4542.

(8) Zhan, X.; Zhu, D. Conjugated polymers for high-efficiency organic photovoltaics. *Polym. Chem.* **2010**, *1*, 409−419.

(9) Facchetti, A. π-Conjugated Polymers for Organic Electronics and Photovoltaic Cell Applications. *Chem. Mater.* **2011**, *23* (3), 733−758.

(10) Yang, J.-S.; Swager, T. M. Fluorescent Porous Films as TNT Chemosensors: Electronic and Structural Effects. *J. Am. Chem. Soc.* **1998**, *120* (46), 11864−11873.

(11) McQuade, D. T.; Pullen, A. E.; Swager, T. M. Conjugated Polymer-Based Chemical Sensors. *Chem. Rev.* **2000**, *100* (7), 2537−2574.

(12) Thomas, S. W.; Joly, G. D.; Swager, T. M. Chemical Sensors Based on Amplifying Fluorescent Conjugated Polymers. *Chem. Rev.* **2007**, *107* (4), 1339−1386.

(13) Xu, B.; Wu, X.; Li, H.; Tong, H.; Wang, L. Selective Detection of TNT and Picric Acid by Conjugated Polymer Film Sensors with Donor-Acceptor Architecture. *Macromolecules* **2011**, *44* (13), 5089−5092.

(14) Chang, C.-C.; Pai, C.-L.; Chen, W.-C.; Jenekhe, S. A. Spin coating of conjugated polymers for electronic and optoelectronic applications. *Thin Solid Films* **2005**, *479*, 254−260.

(15) Zhao, K.; Yu, X.; Li, R.; Amassian, A.; Han, Y. Solvent-dependent self-assembly and ordering in slow-drying drop-cast conjugated polymer films. *J. Mater. Chem. C* **2015**, *3* (38), 9842−9848.

(16) Kim, Y.-J.; Lee, S.; Niazi, M. R.; Hwang, K.; Tang, M.-C.; Lim, D.-H.; Kang, J.-S.; Smilgies, D.-M.; Amassian, A.; Kim, D.-Y. Systematic study on morphological development of blade-coated conjugated polymer thin films via in situ measurements. *ACS Appl. Mater. Interfaces* **2020**, *12* (32), 36417−36427.

(17) Brandão, L.; Viana, J. C.; Bucknall, D. G.; Bernardo, G. Solventless processing of conjugated polymers—A review. *Synth. Met.* **2014**, *197*, 23−33.

(18) Baklar, M. A.; Koch, F.; Kumar, A.; Domingo, E. B.; Campoy-Quiles, M.; Feldman, K.; Yu, L.; Wobkenberg, P.; Ball, J.; Wilson, R. M.; McCulloch, I.; Kreouzis, T.; Heeney, M.; Anthopoulos, T.; Smith, P.; Stingelin, N. Solid-state processing of organic semiconductors. *Adv. Mater.* **2010**, *22* (35), 3942−3947.

(19) Liu, W.; Lei, Z.; Yang, R.; Xing, W.; Tao, P.; Shang, W.; Fu, B.; Song, C.; Deng, T. Facile approach to enhance electrical and thermal performance of conducting polymer PEDOT:PSS films via hot pressing. *ACS Appl. Mater. Interfaces* **2022**, *14* (8), 10605−10615.

(20) Chiong, J. A.; Michalek, L.; Peña-Alcántara, A. E.; Ji, X.; Schuster, N. J.; Bao, Z. Degradable semiconducting polymers without long-range order for on-demand degradation of transient electronics. *J. Mater. Chem. C* **2023**, *11* (43), 15205−15214.

(21) Barik, S.; Skene, W. G. A fluorescent all-fluorene polyazomethine—towards soluble conjugated polymers exhibiting high fluorescence and electrochromic properties. *Polym. Chem.* **2011**, *2* (5), 1091−1097.

(22) Murakami, H.; Kobayashi, K.; Suzuki, K.; Yasuda, T.; Kanbara, T.; Kuwabara, J. Synthesis of azine-based conjugated polymers by metal-free dehydration polycondensation and characterization of their physical properties. *Macromolecules* **2021**, *54* (24), 11281−11288.
(23) Soman, B.; Go, Y. K.; Shen, C.; Leal, C.; Evans, C. M. Impact of dynamic covalent chemistry and precise linker length on crystallization kinetics and morphology in ethylene vitrimers. *Soft Matter* **2022**, *18*, 293−303.
(24) Denissen, W.; Droesbeke, M.; Nicolaÿ, R.; Leibler, L.; Winne, J. M.; Du Prez, F. E. Chemical control of the viscoelastic properties of vinylogous urethane vitrimers. *Nat. Commun.* **2017**, *8*, No. 14857.
(25) Ono, T.; Fujii, S.; Nobori, T.; Lehn, J.-M. Optodynamers: expression of color and fluorescence at the interface between two films of different dynamic polymers. *Chem. Commun.* **2007**, *43*, 4360−4362.
(26) Melchiorre, G.; Visieri, L.; Valentini, M.; Cacciapaglia, R.; Casnati, A.; Baldini, L.; Berrocal, J. A.; Di Stefano, S. Imine-Based Transient Supramolecular Polymers. *J. Am. Chem. Soc.* **2025**, *147* (13), 11327−11335.
(27) Hogg, J. L.; Jencks, D. A.; Jencks, W. P. Catalysis of transamination through trapping by acids and bases. *J. Am. Chem. Soc.* **1977**, *99* (14), 4772−4778.
(28) Qian, X.; Qiu, J.; Hu, B.; Yao, J.; Zuo, M.; Wu, Z.; Shan, G.; Song, Y.; Zheng, Q.; Peng, B.; Li, H.; Du, M. Metal-Like Conductivity in Acid-Treated PEDOT:PSS Films: Surpassing 15,000 S cm^{-1}. *ACS Appl. Mater. Interfaces* **2025**, *17* (11), 17164−17178.
(29) He, S.; Mukaida, M.; Kirihara, K.; Lyu, L.; Wei, Q. Reversible Protonic Doping in Poly(3,4-Ethylenedioxythiophene). *Polymers* **2018**, *10* (10), No. 1065.
(30) Chiang, J.-C.; MacDiarmid, A. G. 'Polyaniline': Protonic Acid Doping of the Emeraldine Form to the Metallic Regime. *Synth. Met.* **1986**, *13* (1−3), 193−205.
(31) Krinichnyi, V. I.; Roth, H.-K.; Schrödner, M.; Wessling, B. EPR study of polyaniline highly doped by p-toluenesulfonic acid. *Polymer* **2006**, *47* (21), 7460−7468.
(32) Nozaki, N.; Uva, A.; Iwahashi, T.; Matsumoto, H.; Tran, H.; Ashizawa, M. Impact of aromatic to quinoidal transformation on the degradation kinetics of imine-based semiconducting polymers. *RSC Appl. Polym.* **2025**, *3* (1), 257−267.
(33) Nitschke, P.; Jarząbek, B.; Bejan, A.-E.; Damaceanu, M.-D. Effect of Protonation on Optical and Electrochemical Properties of Thiophene−Phenylene-Based Schiff Bases with Alkoxy Side Groups. *J. Phys. Chem. B* **2021**, *125* (30), 8588−8600.
(34) Barik, S.; Bletzacker, T.; Skene, W. G. π-Conjugated fluorescent azomethine copolymers: Opto-electronic, halochromic, and doping properties. *Macromolecules* **2012**, *45* (3), 1165−1173.
(35) Sobarzo, P. A.; Jessop, I. A.; Mariman, A. P.; González, A. F.; Saldías, C.; Schott, E.; Zarate, X.; Hauyon, R. A.; Recabarren-Gajardo, G.; González-Henríquez, C. M.; Tundidor-Camba, A.; Terraza, C. A. New thiophene-based poly(azomethine)s bearing tetraphenylsilane moieties along their backbone: Optical, electronic, thermal properties and theoretical calculations. *Eur. Polym. J.* **2020**, *130*, No. 109658.
(36) Altarawneh, S. S.; Max, J. B.; Schacher, F. H.; Ababneh, T. S. Synthesis, characterization, thermodynamics and thermal degradation kinetics of imine-linked polymers. *J. Polym. Res.* **2020**, *27*, No. 349.
(37) Pandey, R. K.; Singh, A. K.; Prakash, R. Directed Self-assembly of Poly(3,3‴-dialkylquarterthiophene) Polymer Thin Film: Effect of Annealing Temperature. *J. Phys. Chem. C* **2014**, *118* (40), 22943−22951.
(38) Son, S. Y.; Kim, Y.; Lee, J.; Lee, G.-Y.; Park, W.-T.; Noh, Y.-Y.; Park, C. E.; Park, T. High-Field-Effect Mobility of Low-Crystallinity Conjugated Polymers with Localized Aggregates. *J. Am. Chem. Soc.* **2016**, *138*, 8096−8103.
(39) Rodrigues, A.; Nabankur, D.; Hilliou, L.; Viana, J.; Bucknall, D. G.; Bernardo, G. Low-temperature solid-state processing of pure P3HT fibers. *AIP Adv.* **2013**, *3* (5), No. 052116.
(40) Ciaccia, M.; Stefano, D. S. Mechanisms of imine exchange reactions in organic solvents. *Org. Biomol. Chem.* **2015**, *13* (3), 646−654.
(41) Snyder, C. R.; Nieuwendaal, R. C.; DeLongchamp, D. M.; Luscombe, C. K.; Sista, P.; Boyd, S. D. Quantifying Crystallinity in High Molar Mass Poly(3-hexylthiophene). *Macromolecules* **2014**, *47* (12), 3942−3950.
(42) Zhao, Y.; Yuan, G. X.; Roche, P.; Leclerc, M. A calorimetric study of the phase transitions in poly(3-hexylthiophene). *Polymer* **1995**, *36* (11), 2211−2214.
(43) Busch, P.; Rauscher, M.; Smilgies, D.-M.; Posselt, D.; Papadakis, C. M. Grazing-incidence small-angle X-ray scattering from thin polymer films with lamellar structures − the scattering cross section in the distorted-wave Born approximation. *J. Appl. Crystallogr.* **2006**, *39*, 433−442.
(44) Huq, A. F.; Ammar, A.; Al-Enizi, A. M.; Karim, A. In-situ orientation and crystal growth kinetics of P3HT in drop cast P3HT:PCBM films. *Polymer* **2017**, *113*, 200−213.
(45) Kukhta, N. A.; Luscombe, C. K. Gaining control over conjugated polymer morphology to improve the performance of organic electronics. *Chem. Commun.* **2022**, *58*, 6982−6997.
(46) Boyle, C. J.; Upadhyaya, M.; Wang, P.; Renna, L. A.; Lu-Díaz, M.; Jeong, S. P.; Hight-Huf, N.; Korugic-Karasz, L.; Barnes, M. D.; Aksamija, Z.; Venkataraman, D. Tuning charge transport dynamics via clustering of doping in organic semiconductor thin films. *Nat. Commun.* **2019**, *10* (1), No. 2827.
(47) Chiang, C. K.; Fincher, C. R.; Park, Y. W.; Heeger, A. J.; Shirakawa, H.; Louis, E. J.; Gau, S. C.; MacDiarmid, A. G. Electrical conductivity in doped polyacetylene. *Phys. Rev. Lett.* **1977**, *39* (17), No. 1098.
(48) Diaz, F. R.; Moreno, J.; Tagle, L. H.; East, G. A.; Radic, D. Synthesis, characterization and electrical properties of polyimines derived from selenophene. *Synth. Met.* **1999**, *100*, 187−193.
(49) Tran, H.; Nikzad, S.; Chiong, J. A.; Schuster, N. J.; Peña-Alcántara, A. E.; Feig, V. R.; Zheng, Y.-Q.; Bao, Z. Modular synthesis of fully degradable imine-based semiconducting p-type and n-type polymers. *Chem. Mater.* **2021**, *33* (18), 7465−7474.
(50) Uva, A.; Kim, Y.; Michailovich, S.; Hsu, N. S. Y.; Bain, D. C.; Huang, S. H.; Musser, A. J.; Tran, H. Impact of imine bonds on the electronic properties of degradable carotenoid-based conjugated polymers. *Polym. Chem.* **2025**, *16* (24), 2817−2828.
(51) Kotewicz, K.; Franco, L. R.; Araujo, M.; Wang, E. Acidochromic Behaviors of Indacenodithiophene-Based Conjugated Polymers Containing Azo, Imine, and Vinyl Bonds. *Macromolecules* **2025**, *58* (5), 2719−2729.
(52) Gracia-Fernández, C. A.; Gómez-Barreiro, S.; López-Beceiro, J.; Naya, S.; Artiaga, R. New approach to the double melting peak of poly(L-lactic acid) observed by DSC. *J. Mater. Res.* **2012**, *27* (10), 1379−1382.
(53) Johnson, J. E.; Morales, N. M.; Gorczyca, A. M.; Dolliver, D. D.; McAllister, M. A. Mechanisms of Acid-Catalyzed Z/E Isomerization of Imines. *J. Org. Chem.* **2001**, *66* (24), 7979−7985.
(54) Firth, N. C.; Brown, N.; Blagg, J. Plane of Best Fit: A Novel Method to Characterize the Three-Dimensionality of Molecules. *J. Chem. Inf. Model.* **2012**, *52* (10), 2516−2525.
(55) Lin, A.; Liu, Z.; Upreti, S.; Lo, S.; Hsu, N. S. Y.; Gu, X.; Wang, S.; Tran, H. Degradable Donor-Acceptor Polymeric Mixed Ionic-Electronic Conductors for Transient Electronics. *Adv. Mater. Technol.* **2026**, *11*, No. e02543.
(56) Chen, J.; Cong, S.; Liu, R.; Duan, J.; Chen, C.; Yu, D.; Zhu, X.; Ran, C.; Cheng, D.; Li, Z.; McCulloch, I.; Yue, W. Imine-Based Polymeric Mixed Ionic-Electronic Conductors Featuring Degradability and Biocompatibility for Transient Bioinspired Electronics. *Angew. Chem., Int. Ed.* **2025**, *64*, No. e202417921.

https://doi.org/10.1021/acs.macromol.6c00291
Macromolecules 2026, 59, 9015−9026